crystals

MDPI

Article

Glassy Properties of the Lead-Free Isovalent Relaxor $BaZr_{0.4}Ti_{0.6}O_3$

Cene Filipič [1], Giovanna Canu [2], Raša Pirc [1] and Zdravko Kutnjak [1,3,*]

[1] Jožef Stefan Institute, Jamova Cesta 39, 1000 Ljubljana, Slovenia; cene.filipic@ijs.si (C.F.); rasa.pirc@ijs.si (R.P.)
[2] CNR-ICMATE, Institute of Condensed Matter Chemistry and Technologies for Energy, National Research Council, Via De Marini 6, I-16149 Genoa, Italy; giovanna.canu@cnr.it
[3] Jožef Stefan International Postgraduate School, Jamova Cesta 39, 1000 Ljubljana, Slovenia
* Correspondence: zdravko.kutnjak@ijs.si

Abstract: Glassy dielectric properties were investigated in lead-free $BaZr_{0.4}Ti_{0.6}O_3$ (BZT40) ceramic samples using dielectric spectroscopy in the frequency range of 0.003 Hz–1 MHz and at temperatures of 10 K < T < 300 K. Measurements of the quasistatic dielectric polarization in bias electric fields up to ~28 kV/cm suggested that a ferroelectric state could not be induced, in contrast to the case of canonical relaxors such as PMN. The quasistatic dielectric and freezing dynamics results for the above field amplitudes showed that BZT40 effectively behaves as a dipolar glass. The relaxation spectrum was analyzed employing a frequency–temperature plot, which showed that the longest relaxation time obeyed the Vogel–Fulcher relation $\tau = \tau_0 \exp[E_0/(T - T_0)]$, with a freezing temperature of 76.7 K. The shortest relaxation time, in contrast, was characterized by a freezing temperature value close to 0 K, implying an Arrhenius-type behavior. The higher value of the polarization and the nonlinear third-order dielectric coefficient ε_3 indicated a shift from a pseudospin glass behavior observed for $BaZr_{0.5}Ti_{0.5}O_3$ (BZT50) toward a classical relaxor ferroelectric state.

Keywords: dielectric properties; electronic ceramics; polarization and depolarization; functional properties; relaxor ferroelectrics; PZT ceramics

Citation: Filipič, C.; Canu, G.; Pirc, R.; Kutnjak, Z. Glassy Properties of the Lead-Free Isovalent Relaxor $BaZr_{0.4}Ti_{0.6}O_3$. *Crystals* **2023**, *13*, 1303. https://doi.org/10.3390/cryst13091303

Academic Editor: Maria Gazda

Received: 24 June 2023
Revised: 17 August 2023
Accepted: 18 August 2023
Published: 25 August 2023

1. Introduction

Since the 1960s, relaxor ferroelectrics have remained in the scientific focus because of their exceptional physical properties [1], such as high dielectric permittivity, large polarization and pyroelectricity, and significant electromechanical response [2–7]. Recently, it was shown that they also possess large caloric properties [8–10]. While the former properties benefit from the electric field-induced long-range ferroelectric order, an inherent property of relaxors in contrast to dipolar glasses, the electrocaloric response and wide temperature stability of these properties are enhanced by the disordered glassy nature of these materials [1–4]. Similarly to dipolar glasses at low electric fields, the glassy nature is reflected in the absence of a long-range ferroelectric order, i.e., spontaneous polarization and symmetry change at very low temperatures, formation of polar nanoregions (PNRs) appearing at relatively high temperatures, and broad dispersion of the complex dielectric permittivity. At the freezing temperature, the longest dipolar relaxation time diverges; hence, ergodicity breaking occurs [2,4]. Relaxors such as the disordered perovskite $PbMg_{1/3}Nb_{2/3}O_3$ (PMN) [3] thus exhibit dipolar glass properties below or ferroelectric properties above the critical field line $E_C(T)$ [2–5].

The lead-free $BaZr_xTi_{1-x}O_3$ (BZT) solid solution recently came into focus because of its possible conceptual proximity to magnetic spin glasses; since zirconium is isovalent to titanium, the random fields should be suppressed [11]. Structural investigations of BZT ceramics with various Zr concentrations, x, showed relaxor properties for $0.25 \leq x \leq 0.75$ [12–23]. In a recent review paper, Petzelt et al. [23] presented an infrared-range broadband dielectric study of a whole concentration range of the $(1 - x)BaTiO_{3-x}BaZrO_3$

(BZT-x) solid solution. They found different characteristic composition ranges, which included proper ferroelectric (x = 0), diffuse ferroelectric ($0 < x \leq 0.2$), relaxor ferroelectric ($0.4 \leq x \leq 0.8$), dipolar glass (x > 0.8), and the standard dielectric (x = 1) properties. They concluded that in the relaxor range, the activated hopping process of Ti ions following the Arrhenius law was behind the broad dielectric relaxation in $BaTiO_3$ clusters. Consequently, the relatively small polar nano regions with frozen boundaries did not change with temperature. In contrast, the canonical lead-based relaxors exhibit polar nano regions′ growth on cooling, leading to glass-like freezing.

Theoretical first-principles studies and microscopic modeling [11,24–26] of BZT with $x = 0.50$ indicated the formation of PNRs with a negligible contribution of random electric fields and strains and that BZT could be mapped to a soft pseudospin glass. The concentration $x = 0.50$ was experimentally investigated [15,27,28], raising arguments about whether BZT in the composition range of $0.25 < x < 0.75$ exhibits properties of a lead-free isovalent relaxor or of a dipolar glass.

Our initial BZT50 dielectric spectroscopy study [27], through the Kutnjak or temperature –frequency plot, demonstrated the asymmetric stretching of the relaxation spectrum in which different portions of the spectrum followed the divergent Vogel–Fulcher relation; only the highest frequencies obeyed the Arrhenius equation describing the activated process. However, such behavior can be found for both relaxors and dipolar glasses. Several criteria can be found in the literature to discern between the relaxor and the dipolar glass states. (i) In dipolar glasses, the distribution of the relaxation times $f(\tau)$ is a simple function with a single peak as a consequence of the fact that PNRs in dipolar glasses will remain small, on the scale of a few unit cells. In contrast, PNRs in relaxors, due to their larger size and stronger coupling to the applied electric field, show breathing modes besides the flipping one. This could result in the second peak in $f(\tau)$. The shape of $f(\tau)$ can be extracted from dielectric dispersion data utilizing the so-called Tikhonov regularization method [29–32]. However, in many cases, both processes could be merged into a single peak distribution function, in which the lower frequency glassy tail diverges. At the same time, the high-frequency *breathing* part follows an activated process. (ii) Another criterion exploits the fact that in canonical relaxors like PMN, the electric field could induce a ferroelectric phase via a discontinuous transition [6,33], resulting in box-like hysteresis loops with sharp steps on rising slopes. In contrast, very narrow hysteresis loops can be found in dipolar glasses, and no critical field line $E_C(T)$ can be induced. (iii) The nonlinear third-order dielectric coefficient ε_3 is typically small in dipolar glasses propagating the linear dielectric response to higher fields. In contrast, classical relaxor systems exhibit a larger ε_3, thus showing the nonlinear dielectric response already at modest electric fields.

To verify the impact of Zr reduction on the pseudospin glass state in BZT, the quasistatic and dynamic dielectric properties of BZT at $x = 0.40$ were experimentally determined. BZT40 possesses a lower concentration of Zr compared to the previously studied BZT50 ceramic and is thus closer to the lower limit of the relaxor regime approaching the ferroelectric one. The standard methods of monitoring the field-cooled quasistatic polarization on cooling, testing the nonlinearity of polarization loops as well as the possible existence of the critical field line $E_C(T)$, were employed to establish the nature of the ordering in BZT40 [34].

2. Materials and Methods

Powders of BZT with $x = 0.40$ were synthesized using the same route as that for the BZT50 samples, i.e., a solid-state reaction [35]. The precursors were calcinated in stoichiometric amounts at 1273 K for 4 h [35]. The powder was compacted at 1500 bar using cold isostatic pressing and sintered at 1773 K for 4 h [35]. The obtained ceramics with a relative density above 99% had a single-phase perovskite structure and a grain size of a few microns [18,27]. We cut 0.26 mm thick ceramics samples from pellets of 6 mm diameter, and gold electrodes of 5 mm diameter were sputtered on the pellet surfaces.

The complex dielectric permittivity $\varepsilon * (f, T) = \varepsilon' - i\varepsilon''$ was measured in the temperature interval from 10 K to 300 K and in the range of frequencies 0.003 Hz < f < 1 MHz by a Novocontrol Technologies Beta High Performance Impedance Analyzer capable to reliably measure the dielectric permittivity in the frequency range from 20 MHz to μHz. The peak-to-peak amplitude of the measuring AC electric field was 10 V/cm. An Oxford Instruments Limited continuous-flow cryostat operating between 1.5 K and 500 K and an ITC4 temperature controller were used to stabilize the temperature within ±0.1 K.

The quasistatic dielectric polarization $P(T, E)$ was measured in field-cooled (FC) and zero-field-heated (ZFH) runs via the charge-collection technique [27,33]. The induced FC (or ZFH) polarization charge by various external dc bias fields (from 5 kV/cm to 28 kV/cm) was collected by a Keithley 6517B programmable Electrometer/High Resistance Meter [36]. The cooling (FC) or heating rate (ZFH) of 1.6 K/min was used. The FC polarization was measured on cooling in the external field down to 10 K, where the external field had been removed from the sample, and on heating, the ZFH quasistatic dielectric polarization was determined.

Virgin $P(E)$ branches were determined by a homemade Sawyer–Tower bridge and a Keithley 6517B programmable electrometer. The period of the external AC electric field, changing from 0 kV/cm to 28 kV/cm and back, was approximately 500 s. The $P(E)$ branches were measured at a specific temperature after annealing the sample at room temperature in the absence of the electric field to remove any history effects.

3. Results and Discussion

Figures 1 and 2 show the ε' and ε'' as functions of the temperature in the range of frequencies of 0.003 Hz–1 MHz. Such typical variation is found in dipolar glasses or relaxors with an increasing shift of the temperature position of the peak with decreasing frequency. Figure 3 shows the frequency f as a function of the temperature T at which $\varepsilon''(f, T)$ achieved its maximum value. The frequency f was found to follow the Vogel–Fulcher (VF) relation

$$f = f_0 \exp\left[-\frac{E_0}{T - T_0}\right]. \quad (1)$$

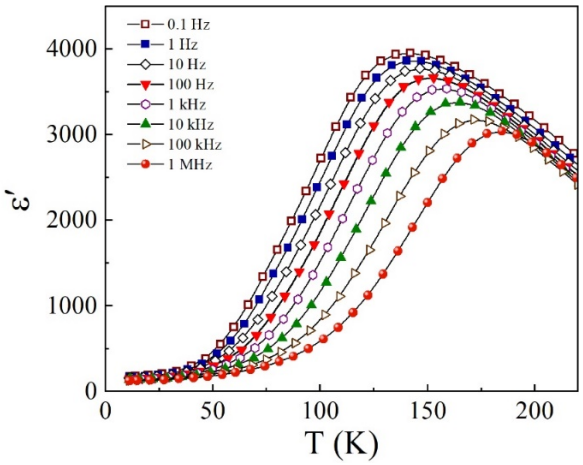

Figure 1. Typical relaxor-like diffuse frequency-dependent peaks of the real part of the dielectric permittivity ε' in BZT40.

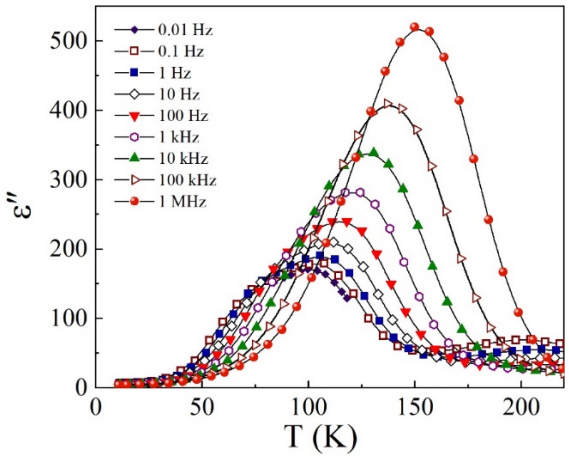

Figure 2. ε'' as a function of the temperature in BZT40 at different frequencies.

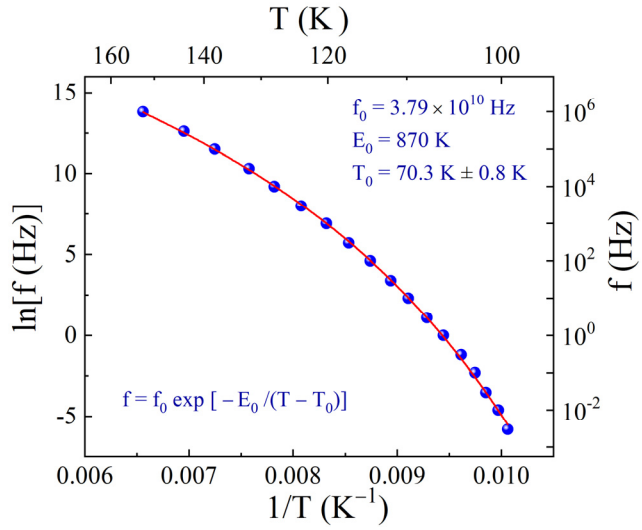

Figure 3. The frequency f as a function of the temperature T at which $\varepsilon''(f, T)$ exhibits its maximum value (solid circles). The solid line is a fitting curve using Equation (1).

Here, f_0 =3.79 × 10^{10} Hz is the attempt frequency, E_0 =870 K represents the VF activation energy, and T_0 = 70.3 K ± 0.8 K is the VF freezing temperature [37]. The interpretation of T_0 as the freezing temperature T_F in the static limit is not unique because ε' and ε'' provided a slightly different value for T_0, as the temperature positions of $\varepsilon''(f, T)$ and $\varepsilon''(f, T)$ diffuse peaks did not match (see Figure 1).

A comparison of the dielectric data observed for BZT50 [27] and BZT40 showed that these two sets of data were qualitatively quite similar, with the dispersive temperature dependence of the real and imaginary part of dielectric permittivity whose peaks followed the Vogel–Fulcher relation. By lowering the Zr content from x = 0.5 to x = 0.4, the dielectric peaks were shifted to higher temperatures for about 60 K, increasing the dielectric values by about 50%. Consequently, the T_0 increased from 9.5 K to 70.3 K, the attempt frequency f_0 decreased of about three orders of magnitude (4.08 × 10^{13} Hz to 3.79 × 10^{10} Hz), while the VF activation energy E_0 decreased from 2255 K to 870 K. These observations indicated the approach of the ferroelectric regime as the Zr content decreased.

The so-called Cole–Cole diagram (Figure 4) in which ε'' is parametrically plotted as a function of ε' could reveal the static and high-frequency limits of the dielectric relaxation as well as the asymmetry of the relaxation spectrum. The increasing asymmetric shape and strong suppression of the dispersion with the decreasing temperature indicated a strong asymmetric broadening of the relaxation spectrum. The Havriliak–Negami (HN) function

was employed to extract the static dielectric permittivity, ε_S, and the high-frequency limit, ε_∞,

$$\varepsilon * (\omega, T) = \varepsilon_\infty + \frac{\varepsilon_s - \varepsilon_\infty}{\left[1 + (i\omega\tau)^\alpha\right]^\beta}, \quad (2)$$

where $\omega = 2\pi f$, and τ is the characteristic relaxation time. Examples of the fits are shown in the inset of Figure 4, with the fitting parameters presented in Table 1.

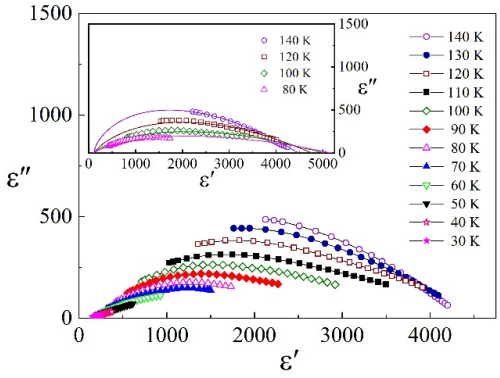

Figure 4. The parametric ε'' vs. ε' plots for BZT40 at temperatures from 30 K to 140 K. Representative fits with the HN function are shown in the inset. Here, the solid lines represent the fitting curves with the parameters shown in Table 1.

Table 1. The fitting parameters for the fitting curves shown in the inset of Figure 4.

T (K)	ε_S	ε_∞	α	β	f = 1/τ (s^{-1})
140	4482.9	121.1	0.198	34.4	1.2×10^{14}
120	4768.5	115.7	0.147	5.34	7.5×10^{10}
100	5036.4	109.3	0.095	5.0	1.6×10^{10}
80	5192	103.6	0.073	4.9	5.2×10^{7}

Figure 5 shows the static ε_S and high-frequency limit ε_∞ fitting parameters as functions of the temperature. As the dielectric dispersion could not be covered with experimentally available frequencies, the fitting procedure allowed the estimation of the temperature dependence of ε_s, ε_∞, and τ in a relatively narrow range of temperatures. Fortunately, it was shown before that the static dielectric permittivity ε_S coincides with the quasistatic dielectric value ε_{FC}, determined in the FC run at a low electric field [27,37,38].

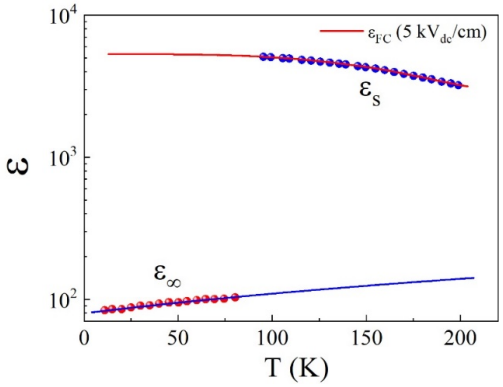

Figure 5. ε_S and high-frequency ε_∞ dielectric permittivities as functions of the temperature in BZT40. The solid circles represent the fitting parameters determined by fitting the experimental data to the HN function. The solid lines represent the guides to the eye.

The temperature–frequency plot introduced in Ref. [37] allows the observation of how various segments of the relaxation times distribution function vary with the temperature. The data analysis procedure via the temperature–frequency plot is described in detail in Refs. [37–39]. The temperature–frequency plot exploits a special presentation of the real part of the complex dielectric permittivity that provides direct information on the temperature evolution of the relaxation spectrum. In this method, it is presumed that the relaxation spectrum is broad but limited, i.e., constrained between the upper and the lower relaxation time cut-offs. The special presentation of the real part of the complex dielectric permittivity is introduced through the parameter $\delta = \delta(\omega,\ T)$ or the reduced dielectric permittivity, defined as

$$\delta(\omega,\ T) = \frac{\varepsilon'(\omega,\ T) - \varepsilon_\infty}{\varepsilon_s - \varepsilon_\infty} = \int_{z_1}^{z_2} \frac{g(z)dz}{1 + (\omega/\omega_a)^2 \exp(2z)}, \tag{3}$$

where $z = \log(\omega_a \tau)$, ω_a is an arbitrary unit frequency, and z_1 and z_2 represent the limits of the distribution of the relaxation times [38,39]. The right part of Equation (3) can be considered the filter $1/1 + (\omega/\omega_a)^2 \exp(2z)$ acting upon the distribution of the relaxation times $g(z)$ that opens at $z \approx \ln(\omega_a/\omega)$. In the case of a broad distribution of the relaxation times, the value of the integral in Equation (3) is determined for low values of $\varepsilon'(\omega,\ T)$ or $\delta \approx 0$ by contributions stemming from the short τ (high-frequency) part of $g(z)$. In contrast, for values of ε' close to the static dielectric permittivity ε_s or $\delta \approx 1$, the whole distribution of the relaxation times $g(z)$ contributes to the integral in Equation (3); thus, the frequency filter probes the shape of $g(z)$ near its long relaxation time (low frequency) cut-off z_2. Therefore, by scanning δ from 0 to 1, the filter in the second part of Equation (3) probes the distribution of the relaxation times $g(z)$ by shifting its position in τ space. The position of the frequency filter can be used as a probe to discern the changes in the shape or polydispersity of the relaxation spectrum. Consequently, δ, which can be estimated directly from the dielectric permittivity data, actually represents contributions of $g(z)$ for relaxation times below $1/\omega$. In the analysis, δ is taken as an independent parameter whose value is set to some fixed values between 0 and 1. Technically, for the chosen set of fixed values of δ at a given temperature, the corresponding set of frequency values $f = \omega/2\pi$ was determined by a suitable interpolation technique between the discrete experimental points at which a given ε' was realized. It should be stressed again that scanning ε' between ε_S and ε_∞ changed uniquely δ from 1 to 0. The set of frequencies can also be determined from Figure 1 as cross sections between the experimental data $\varepsilon'(\omega, T)$ curves and the $\varepsilon' = const$ ($\delta = const$) lines. Figure 6 presents $\ln(f)$ vs. $1/T$ for δ values in the range of $0.05 < \delta < 0.98$.

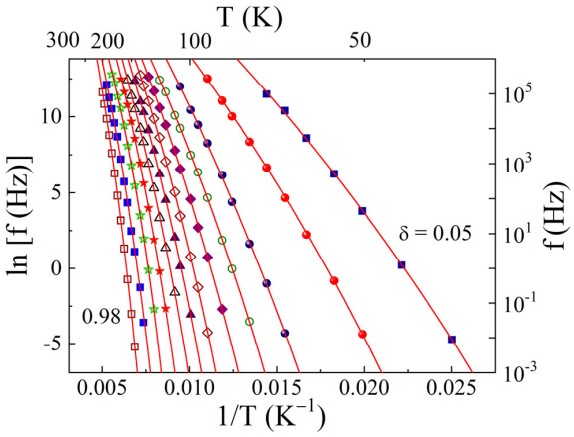

Figure 6. Temperature–frequency plots representing the temperature evolution of various segments of the distribution of the relaxation times, measured by the reduced dielectric permittivity δ top to bottom, 0.05, 0.10, 0.20, 0.30, 0.40, 0.50, 0.60, 0.70, 0.80, 0.90, 0.95, 0.98. The temperature evolution of each relaxation spectrum segment denoted by δ was fitted to a VF ansatz (solid lines).

The temperature variation of different parts of the relaxation spectrum related to various δ could be extracted by fitting each curve with a VF ansatz

$$f_\delta = f_{0\delta}\exp\left[-\frac{E_\delta}{T - T_{0\delta}}\right], \quad (4)$$

where δ runs over values representing each curve in Figure 6 [37]. Thus, the obtained freezing temperatures for different parts of the relaxation spectrum, i.e., the different values of δ are depicted in Figure 7. The longest $1/f_2$ and the shortest relaxation time $1/f_1$ correspond to the limiting cases $\delta \to 1$ and $\delta \to 0$, respectively. Figure 7 also shows T_0 vs. δ in BZT50 [27]. The fitting parameters for the relaxation spectrum cut-off frequencies f_1 and f_2 are listed in Table 2 for both BZT40 and BZT50 ceramics. It should be noted that, according to the experimental time scale, the value T_0 = 70.3 K obtained from the dispersion of $\varepsilon''(f, T)$ peaks (see Figure 3) roughly matched the freezing temperature denoted by $\delta \approx 0.95$. It should be noted that the above analysis was possible only in the temperature range in which ε_S and ε_∞ were well established.

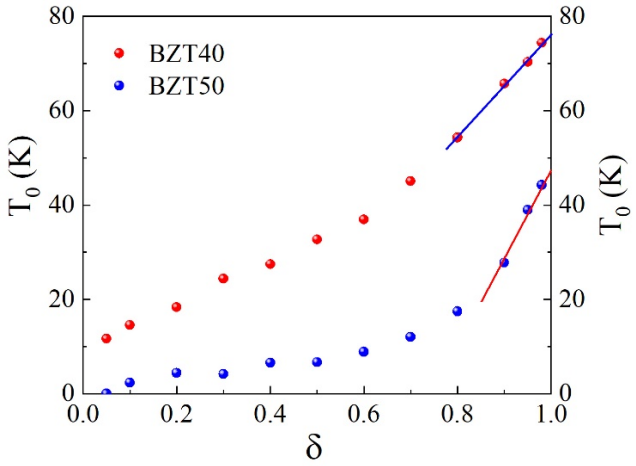

Figure 7. Freezing temperature T_0 vs. δ for BZT40 (red circles). The solid line is an extrapolation to $\delta \to 1$, corresponding to the limit of the longest relaxation times. The blue circles represent $T_0(\delta)$ in BZT50 [27].

Table 2. The fitting parameters for the relaxation spectrum cut-off frequencies f_1 and f_2 for BZT40 and BZT50 ceramics.

Sample	Cut-off Frequencies	T_0 (K)	E_0 (K)	f_0 (Hz)
BZT40	$f_1(\delta \to 0)$	11.6	910	7.78×10^{11}
	$f_2(\delta \to 1)$	74.4	2790	5.67×10^{14}
BZT50	$f_1(\delta \to 0)$	≈0	1330	2.17×10^{14}
	$f_2(\delta \to 1)$	48.1	725	3.65×10^{5}

The impact of freezing dynamics is best manifested in the stark difference between FC and ZFH polarization [2,37]. The splitting of the quasistatic FC and ZFH (after field-cooling) polarization is shown in Figure 8, measured at the dc electric field of 28 kV/cm. The difference between the FC and the ZFH curves at the lowest temperatures is due to the fast high-frequency relaxation of the polarization, i.e., to fast processes contributing to ε_∞. From $\varepsilon_\infty = (P_{FC} - P_{ZFH})/\varepsilon_\infty E$, the dielectric dispersion high-frequency limit $\varepsilon_\infty = 90$ could be estimated in agreement with the HN function analysis value (see Figure 5). P_{ZFH}

or the remanent polarization P_r was detected after removing the external electric field at 10 K, after the FC experiment.

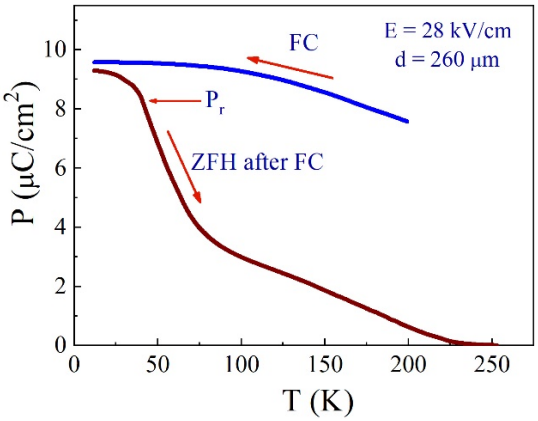

Figure 8. The quasistatic FC (blue curve) and ZFH (or P_r measured after a field-cooled run) (red curve) polarization as a function of temperature. The FC curve was obtained in the 28 kV/cm electric field. The temperature $T_{02} = 74.4$ K corresponds to the temperature of the knee in the $P_r(T)$ slope variation.

Figure 8 shows that P_{ZFH} or P_r were almost unchanged to the temperature $T_F \approx 50$ K, after which the P_r rapidly started to decrease because, above 50 K, most of the relaxation spectrum shifted back into the experimental time window. P_r relaxed fast toward the longest relaxation time's freezing temperature $T_{02} = 74.4$ K, at which the steepest slope in $P_r(T)$ variation changed, followed by a slowly decreasing shoulder, which vanished at ≈225 K (see Figure 8). In contrast to T_{02}, the freezing temperature $T_F \approx 50$ K depends on the experimental time scale and cannot be considered a true static quantity. The shift of T_{02} to higher temperatures and the long polarization tail persisting to high temperatures (Figure 8) indicated the shift of the BZT40 state from a pseudospin-glass state [9] toward the classical relaxor-type behavior. A similar shift was found recently in another isovalent relaxor system, $BaTi_{1-x}Ce_xO_3$, where the composition x = 0.30 showed dipolar glass properties in contrast to the composition x = 0.20 with relaxor ferroelectric properties [40,41].

To investigate the nonlinear properties of the induced polarization $P(E)$, the quasistatic electric external field was cycled from 0 kV/cm up to 28 kV/cm at a low frequency of ≈0.002 Hz. In a typical relaxor, like PMN, "slim" nonlinear polarization loops with negligibly small remanent polarization are usually observed in a portion of the electric field–temperature ($E - T$) phase diagram near or for temperatures above the freezing line (dashed line in Figure 9) [33].

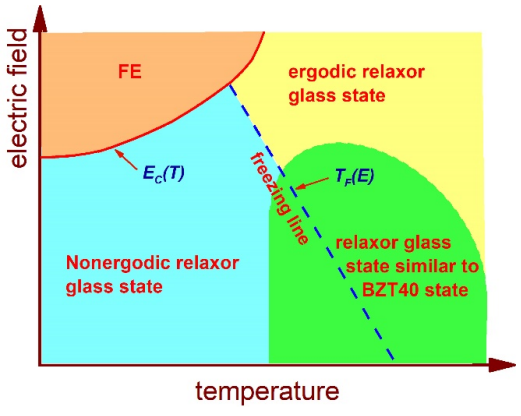

Figure 9. E–T phase diagram of a classical relaxor system like PMN. The green area marks the portion of the phase diagram with similar dielectric properties as those observed for BZT40.

At temperatures below the freezing line, "square" loops were observed at fields above the critical threshold to induce the ferroelectric phase [33]. In the region above the freezing temperature line $T_F(E)$ (dashed line in Figure 9), polar nanoclusters appeared as fluctuating entities, and P_r remained nearly zero; however, $P(E)$ remained strongly nonlinear [33,42]. By contrast, the field could not induce large domains in dipolar glasses, and single dipoles or very small dipolar clusters remained the only relaxing entities. Such a state resembled a paraelectric state characterized by linear properties, with a small third-order nonlinear dielectric coefficient, ε_3. The remanent polarization resembled frozen polar clusters oriented in the external electric field, which, below the freezing temperature, remained ordered even after the field was turned off.

Figure 10 shows the induced polarization $P(E)$ as a function of the applied field at different temperatures above the freezing temperature of 74.4 K. The polarization was measured by increasing and subsequently decreasing the field from 0 to 28 kV/cm within the 500 s experimental time scale. The application of a negative electric field reproduced symmetric negative polarization branches. The experimental time scale could be considered quasistatic in the temperature range above 80 K. Here, quasistatic "loops" did not show any hysteresis, as shown in Figure 10, where both up and down $P(E)$ data lie on the same curve, i.e., the remanent polarization is zero. Due to the increasing longest relaxation times at lower temperatures, the data obtained when decreasing the field could not relax within the experimental time scale back to the initial values, resulting in artificial dynamic hysteresis. It was verified that this dynamic hysteresis disappeared if the time scale of the experiment increased. Verification was carried out up to the 2000 sec time scale. The observed maximum polarization of 10 μC/cm^2 at 28 kV/cm exceeded almost by a factor of 2 the polarization observed in the same field of 28 kV/cm in BZT50 (5.5 μC/cm^2). The nonlinearity of the $P(E) = \varepsilon_0\varepsilon_1 E + \varepsilon_3 E^3 + \varepsilon_5 E^5$ was strong, with the absolute value of the otherwise negative third-order nonlinear dielectric coefficient $-\varepsilon_3 = 2\times10^{-21}$ AsV^{-3}m at 225 K increasing toward $-\varepsilon_3 = 4\times10^{-21}$ AsV^{-3}m at 80 K, i.e., with the temperature approaching the freezing temperature. The absolute value of the third-order nonlinear dielectric coefficient ε_3 for BZT40 was about one order of magnitude larger than that for BZT50 [27]. The nonlinearity increased with the decreasing temperature, indicating the approaching onset of the long-range ferroelectric order. The experimentally limited maximum field of 28 kV/cm was insufficient to induce a ferroelectric phase, and the question remains whether a long-range ferroelectric order could be induced in BZT40.

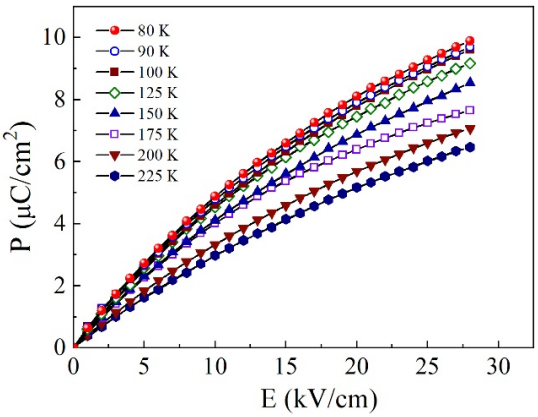

Figure 10. The nonlinearity of $P(E)$ in BZT40 at various temperatures above the freezing temperature. The figure shows data from both 0-to-28 kV/cm and reverse runs.

Figure 11 shows the temperature dependence of the linear dielectric permittivity $\varepsilon''(f,T)$ determined in the range of frequencies from 0.1 Hz to 1 MHz in a low electric field of 10 V/cm and ε_{FC}, obtained in an FC run with a dc field of 5 kV/cm, below which $P(E)$ is still linear (see Figure 10), thus allowing the calculation of the linear dielectric permittivity

$\varepsilon_{FC} = P_{FC}/\varepsilon_0 E$ from the measured P_{FC}. The static dielectric permittivity obtained from HN function fits (red circles) agreed well with the quasistatic ε_{FC} obtained from the FC experiments, thus allowing the determination of the static dielectric permittivity at temperatures below the freezing temperature, i.e., in the temperature range experimentally inaccessible by established dielectric techniques.

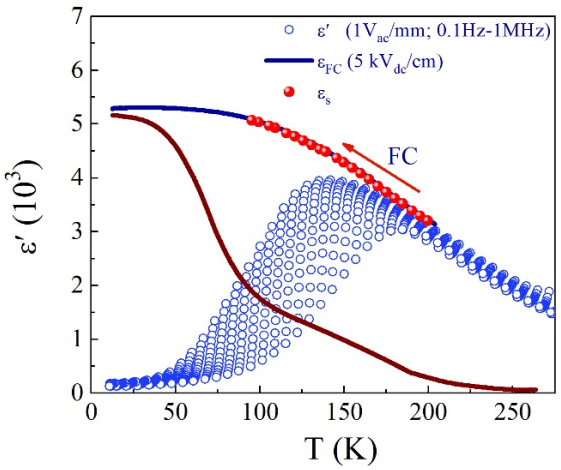

Figure 11. Temperature variation of the dielectric permittivity $\varepsilon''(f,T)$ (open blue circles), $\varepsilon_{FC} = P_{FC}/\varepsilon_0 E$, obtained in a field-cooled (FC) experiment (solid blue line) and ε_S (solid red circles) obtained from the Cole–Cole plots (c.f. Figure 5). The red curve represents ZFH or P_r measured after a field-cooled run.

4. Conclusions

This dielectric spectroscopy study was performed to verify the dynamic and quasistatic dielectric properties of isovalent relaxor BZT40 ceramics. Dielectric spectroscopy in the frequency range 0.003 Hz–1 MHz and at temperatures of 10 K < T < 300 K revealed, via temperature–frequency plot analysis, that different parts of the relaxation spectrum followed the Vogel–Fulcher law. Only the very high-frequency part behaved according to the Arrhenius-activated process. The maximum relaxation time was found to diverge at the freezing temperature of 74.4 K. Such features were observed in both pseudospin glass and relaxor ferroelectric systems. The quasistatic dielectric polarization $P(E)$ measured in an FC experiment was about two times larger than that of BZT50, measured in the same field of 28 kV/cm. Consequently, the quasistatic dielectric permittivity $\varepsilon_{FC} = 5300$, measured in the linear regime, was also twice larger than in BZT50. In addition, the polarization field dependence $P(E)$ was more strongly nonlinear than in BZT50, with the absolute value of the third-order nonlinear dielectric coefficient $\varepsilon_3 = -4 \times 10^{-21}$ AsV^{-3}m being ten times larger than that of BZT50. Up to 28 kV/cm, however, no transition to a ferroelectric-ordered state could be induced.

The higher dielectric permittivity $P(E)$ and the third-order dielectric nonlinearity ε_3 suggest that BZT40 ceramics exhibit a crossover from the *incipient* relaxor state, i.e., the state closer to the pseudospin glass found in BZT50 ceramics, towards the diffuse ferroelectric (relaxor) state observed in BZT compositions with $0 < x \leq 0.2$. The high values of the above physical quantities observed in BZT40 are typical properties of classical relaxors like PMN. In contrast to PMN and similar to BZT50, the electric field could not induce the ferroelectric state and had no substantial influence on dipolar dynamics in BZT40 ceramics.

Author Contributions: Conceptualization, C.F. and Z.K.; methodology, Z.K.; formal analysis, C.F. and Z.K.; investigation, C.F. and Z.K.; resources, G.C.; data curation, C.F.; writing—original draft preparation, C.F. and Z.K.; writing—review and editing, C.F., R.P., G.C. and Z.K.; visualization, C.F. and Z.K.; supervision, R.P.; project administration, Z.K.; funding acquisition, Z.K. All authors have read and agreed to the published version of the manuscript.

Funding: This work was supported by the Slovenian Research and Innovation Agency under the programs P1-0125 and P1-0044.

Data Availability Statement: The data that support the findings of the study are available within this article.

Acknowledgments: The authors thank J. Petzelt for the discussion and feedback in the early stages of the study.

Conflicts of Interest: The authors declare no conflict of interest.

References

1. Blinc, R. *Advanced Ferroelectricity*; Oxford University Press: New York, NY, USA, 2011.
2. Levstik, A.; Kutnjak, Z.; Filipič, C.; Pirc, R. Glassy freezing in relaxor ferroelectric lead magnesium niobate. *Phys. Rev. B* **1998**, *57*, 11204–11211. [CrossRef]
3. Smolenskii, G.A.; Isupov, V.A. New Ferroelectrics of Complex Composition IV. *Dokl. Akad. Nauk SSSR* **1954**, *97*, 653.
4. Cross, L.E. Relaxor ferroelectrics: An overview. *Ferroelectrics* **1994**, *151*, 305–320.
5. Samara, G.A. *Solid State Physics*; Ehrenreich, H., Spaepen, R., Eds.; Academic Press: New York, NY, USA, 2001; Volume 56, p. 1.
6. Kutnjak, Z.; Petzelt, J.; Blinc, R. The giant electromechanical response in ferroelectric relaxors as a critical phenomenon. *Nature* **2006**, *441*, 956. [CrossRef]
7. Baasandorj, L.; Chen, Z. Recent Developments on Relaxor-$PbTiO_3$ Ferroelectric Crystals. *Crystals* **2022**, *12*, 56. [CrossRef]
8. Uršič, H.; Vrabelj, M.; Otoničar, M.; Fulanović, L.; Rožič, B.; Kutnjak, Z.; Bobnar, V.; Malič, B. Influence of synthesis-related microstructural features on the electrocaloric effect for $0.9Pb(Mg_{1/3}Nb_{2/3})O_3{}^{-}0.1PbTiO_3$ ceramics. *Crystals* **2021**, *11*, 372. [CrossRef]
9. Kutnjak, Z.; Rožič, B.; Pirc, R. *Electrocaloric Effect: Theory, Measurements, and Applications*; Wiley, Encyclopedia of Electrical and Electronics Engineering; Wiley: Hoboken, NJ, USA, 2015; pp. 1–19.
10. Rožič, B.; Kosec, M.; Uršič, H.; Holc, J.; Malič, B.; Zhang, Q.M.; Blinc, R.; Pirc, R.; Kutnjak, Z. Influence of the critical point on the electrocaloric response of relaxor ferroelectrics. *J. Appl. Phys.* **2011**, *110*, 064118. [CrossRef]
11. Sherrington, D. BZT: A Soft Pseudospin Glass. *Phys. Rev. Lett.* **2013**, *111*, 227601. [CrossRef]
12. Farhi, R.; El Marssi, M.; Simon, A.; Ravez, J. A Raman and dielectric study of ferroelectric ceramics. *Eur. Phys. J. B* **1999**, *9*, 599–604. [CrossRef]
13. Maiti, T.; Guo, R.; Bhalla, A.S. Structure-Property Phase Diagram of $BaZr_xTi_{1-x}O_3$ System. *J. Am. Ceram. Soc.* **2008**, *91*, 1769–1780. [CrossRef]
14. Maiti, T.; Guo, R.; Bhalla, A.S. Electric field dependent dielectric properties and high tenability of $BaZr_xTi_{1-x}O_3$ relaxor ferroelectrics. *Appl. Phys. Lett.* **2006**, *89*, 122909. [CrossRef]
15. Maiti, T.; Guo, R.; Bhalla, A.S. The evolution of relaxor behavior in Ti^{4+} doped $BaZrO_3$ ceramics. *J. Appl. Phys.* **2006**, *100*, 114109. [CrossRef]
16. Maiti, T.; Guo, R.; Bhalla, A.S. Evaluation of Experimental Resume of $BaZr_xTi_{1-x}O_3$ with Perspective to Ferroelectric Relaxor Family: An Overview. *Ferroelectrics* **2011**, *425*, 4–26. [CrossRef]
17. Petzelt, J.; Nuzhnyy, D.; Bovtun, V.; Kempa, M.; Savinov, M.; Kamba, S.; Hlinka, J. Lattice dynamics and dielectric spectroscopy of BZT and NBT lead-free perovskite relaxors—Comparison with lead-based relaxors. *Phase Transit.* **2014**, *88*, 320–332. [CrossRef]
18. Petzelt, J.; Nuzhnyy, D.; Savinov, M.; Bovtun, V.; Kempa, M.; Ostapchuk, T.; Hlinka, J.; Canu, G.; Buscaglia, V. Broadband Dielectric Spectroscopy of $Ba(Zr,Ti)O_3$: Dynamics of Relaxors and Diffuse Ferroelectrics. *Ferroelectrics* **2014**, *469*, 14–25. [CrossRef]
19. Nuzhnyy, D.; Petzelt, J.; Savinov, M.; Ostapchuk, T.; Bovtun, V.; Kempa, M.; Hlinka, J.; Buscaglia, V.; Nanni, P. Broadband dielectric response of $Ba(Zr,Ti)O_3$ ceramics: From incipient via relaxor and diffuse up to classical ferroelectric behaviour. *Phys. Rev. B* **2012**, *86*, 014106. [CrossRef]
20. Kleemann, W.; Miga, S.; Dec, J.; Zhai, J. Crossover from ferroelectric to relaxor and cluster glass in $BaTi_{1-x}Zr_xO_3$ (x = 0.25–0.35) studied by non-linear permittivity. *Appl. Phys. Lett.* **2013**, *102*, 232907. [CrossRef]
21. Qian, X.-S.; Ye, H.-J.; Zhang, Y.-T.; Gu, H.; Li, X.; Randall, C.A.; Zhang, Q.M. Giant Electrocaloric Response Over A Broad Temperature Range in Modified $BaTiO_3$ Ceramics. *Adv. Funct. Mater.* **2014**, *24*, 1300–1305. [CrossRef]
22. Kleemann, W.; Dec, J.; Miga, S. The cluster glass route of relaxor ferroelectrics. *Phase Transit.* **2015**, *88*, 234–244. [CrossRef]
23. Petzelt, J.; Bovtun, V.; Nuzhnyy, D.; Kempa, M.; Savinov, M.; Paściak, M.; Kamba, S.; Canu, G.; Buscaglia, V. Broadband Dielectric, Terahertz, and Infrared Spectroscopy of $BaTiO_3$–$BaZrO_3$ Solid Solution: From Proper Ferroelectric over Diffuse and Relaxor Ferroelectrics and Dipolar Glass to Normal Dielectric. *Phys. Status Solidi B* **2021**, *258*, 2100259. [CrossRef]
24. Akbarzadeh, A.R.; Prosandeev, S.; Walter, E.J.; Al-Barakaty, A.; Bellaiche, L. Finite-Temperature Properties of $Ba(Zr,Ti)O_3$ Relaxors from First Principles. *Phys. Rev. Lett.* **2012**, *108*, 257601. [CrossRef]
25. Prosandeev, S.; Wang, D.; Akbarzadeh, A.R.; Dkhil, B.; Bellaiche, L. Field-Induced Percolation of Polar Nanoregions in Relaxor Ferroelectrics. *Phys. Rev. Lett.* **2013**, *110*, 207601. [CrossRef] [PubMed]
26. Prosandeev, S.; Wang, D.; Bellaiche, L. Properties of Epitaxial Films Made of Relaxor Ferroelectrics. *Phys. Rev. Lett.* **2013**, *111*, 247602. [CrossRef] [PubMed]

27. Filipič, C.; Kutnjak, Z.; Pirc, R.; Canu, G.; Petzelt, J. $BaZr_{0.5}Ti_{0.5}O_3$: Lead-free relaxor ferroelectric or dipolar glass. *Phys. Rev. B* **2016**, *93*, 224105. [CrossRef]
28. Wang, D.; Hlinka, J.; Bokov, A.A.; Ye, Z.-G.; Ondrejkovic, P.; Petzelt, J.; Bellaiche, L. Fano resonance and dipolar relaxation in lead-free relaxors. *Nat. Commun.* **2014**, *5*, 5100. [CrossRef] [PubMed]
29. Macutkevic, J.; Banys, J.; Grigalaitis, R.; Visochanskii, Y. Asymmetric phase diagram of mixed $CuInP_2(S_xSe_{1-x})_6$ crystals. *Phys. Rev. B* **2008**, *78*, 064101. [CrossRef]
30. Banys, J.; Grigalaitis, R.; Mikonis, A.; Macutkevich, J.; Keburis, P. Distribution of relaxation times of relaxors: Comparison with dipolar glasses. *Phys. Status Solidi C* **2009**, *6*, 2725–2730. [CrossRef]
31. Bishop, A.R.; Bussmann-Holder, A.; Kamba, S.; Maglione, M. Common characteristics of displacive and relaxor ferroelectrics. *Phys. Rev. B* **2010**, *81*, 064106. [CrossRef]
32. Bussmann-Holder, A. The polarizability model for ferroelectricity in perovskite oxides. *J. Phys. Condens. Matter* **2012**, *24*, 273202. [CrossRef]
33. Kutnjak, Z.; Vodopivec, B.; Blinc, R. Anisotropy of electric field freezing of the relaxor ferroelectric $Pb(Mg_{1/3}Nb_{2/3})O_3$. *Phys. Rev. B* **2008**, *77*, 054102. [CrossRef]
34. Kutnjak, Z.; Pirc, R.; Blinc, R. Field-cooled static nonlinear response of relaxor ferroelectrics. *Appl. Phys. Lett.* **2002**, *80*, 3162. [CrossRef]
35. Buscaglia, V.; Tripathi, S.; Petkov, V.; Dapiaggi, M.; Deluca, M.; Gajović, A.; Ren, Y. Average and local atomic-scale structure in $BaZrxTi_{1-x}O_3$ (x = 0.10, 0.20, 0.40) ceramics by high-energy X-ray diffraction and Raman spectroscopy. *J. Phys. Condens. Matter* **2014**, *26*, 065901. [CrossRef] [PubMed]
36. Levstik, A.; Filipič, C.; Kutnjak, Z.; Levstik, I.; Pirc, R.; Tadić, B.; Blinc, R. Field-cooled and zero-field-cooled dielectric susceptibility in deuteron glasses. *Phys. Rev. Lett.* **1991**, *66*, 2368. [CrossRef] [PubMed]
37. Kutnjak, Z.; Pirc, R.; Levstik, A.; Levstik, I.; Filipič, C.; Blinc, R.; Kind, R. Observation of the freezing line in a deuteron glass. *Phys. Rev. B* **1994**, *50*, 12421. [CrossRef] [PubMed]
38. Kutnjak, Z.; Filipič, C.; Levstik, A.; Pirc, R. Glassy dynamics of $Rb_{0.40}(ND_4)_{0.60}D_2PO_4$. *Phys. Rev. Lett.* **1993**, *25*, 4015. [CrossRef] [PubMed]
39. Kutnjak, Z.; Filipič, C.; Pirc, R.; Levstik, A.; Farhi, R.; El Marssi, M. Slow dynamics and ergodicity breaking in a lanthanum-modified lead zirconate titanate relaxor system. *Phys. Rev. B* **1999**, *59*, 294. [CrossRef]
40. Adamchuk, D.; Grigalaitis, R.; Svirskas, S.; Macutkevic, J.; Palaimiene, E.; Banys, J.; Mitoseriu, L.; Canu, G.; Buscaglia, M.T.; Buscaglia, V. Distributions of relaxation times in relaxor ferroelectric $Ba(Ti_{0.8}Ce_{0.2})O_3$. *Ferroelectrics* **2019**, *553*, 103. [CrossRef]
41. Svirskas, S.; Adamchuk, D.; Grigalaitis, R.; Jablonskas, D.; Macutkevic, J.; Canu, G.; Buscaglia, M.T.; Buscaglia, V.; Curecheriu, L.; Mitoseriu, L.; et al. Dipolar glass state in $BaCe_{0.3}Ti_{0.7}O_3$ perovskite solid solutions. *J. Alloys Compd.* **2021**, *854*, 155755. [CrossRef]
42. Levstik, A.; Bobnar, V.; Filipič, C.; Holc, J.; Kosec, M.; Blinc, R.; Trontelj, Z.; Jagličić, Z. Magnetoelectric relaxor. *Appl. Phys. Lett.* **2007**, *91*, 012905. [CrossRef]